Invited Paper Presented at
61st Canadian Chemical Conference and Exhibition,
Winnipeg, Manitoba, 4-7 June, 1978

VARIOUS APPLICATIONS OF ZEEMAN ATOMIC ABSORPTION SPECTROSCOPY

Hideaki Koizumi *

Lawrence Berekeley Laboratory,
University of California, Berkeley, CA 94720
U.S.A.

ABSTRACT

The application of the Zeeman effect to atomic absorption spectroscopy has been studied over the past several years. This technique has a larger area of application than conventional AAS because of its high degree of selectivity. The ZAA technique can be used for organometallic species determination by interfacing with a high pressure liquid chromatograph. Various kinds of eluents can be directly introduced in the ZAA system; even organic solvents or high concentration salt solutions. For example, the Co atom in the functional center of Vitamin B12 molecule was separately analyzed in the presence of much larger amounts of inorganic Co. In the ZAA technique, interference caused by direct spectral overlap can also be corrected. As a typical example, the Sb line at 217.02 nm overlaps the Pb absorption line at 217.00 nm. However, 1000 ppm of Pb did not cause any interference signal in the Sb analysis by ZAA. This is especially important in the analysis of gun powder residue that is often carried out by chemists working in the forensic field. In the determination of trace elements in matrices of unknown composition, the ZAA technique achieved highly reliable results by employing the standard addition method to correct for chemical interferences, because any non-specific absorption or emission does not give rise to interference signals with this technique.

Introduction

Many years have passed since the discovery of the Zeeman effect in 1897 [1]. Several important fields of research such as the Zeeman assignment of atomic transitions [2], magnetic scanning [3], double resonance [4], etc., depend upon this phenomenon. In the past ten years, the application of the Zeeman effect on atomic absorption spectrometry has been studied by a number of researchers [5]-[25]. Several kinds of techniques, listed in Table 1, were developed. The Zeeman effect was originally applied to atomic absorption spectrometry to correct for the effects of molecular absorption and particulate scattering, i.e., the background absorption. Although the background correction for mercury detection [26] using a continuum source was reported even before Walsh described the atomic absorption spectrometer in 1955 [27], the importance of the background correction was again recognized as interest in electrothermal AA gained ground.

Besides providing highly precise background correction, the Zeeman AA technique provides the optimum arrangement for double beam optics [22]. In addition, it gives excellent correction for interference caused by direct spectral overlap [24]. Increased interest in Zeeman AA techniques is demonstrated by the appearance of several recent reviews of the subject [28]-[30].

In this paper, the author will describe a ZAA instrument based on the Polarized Zeeman AA technique [20], [22], and the following applications will be described: speciation of organometallic compounds, clinical and biological analyses, gun powder residue analysis, highly reliable analysis of the sample with an unknown matrix, high salinity sample analysis, and the determination of minor constituents in steel.

In the magnetic field, the splitting of an atomic energy level into Zeeman components is given by the expression .

$$-\Delta T_M = M \cdot g \cdot L \cdot B \qquad (1)$$

Here, ΔT_M = the change in energy (cm^{-1}) from the 0 field position, B = magnetic induction in gauss, M = the magnetic quantum number, L and g are the Lorentz unit and the Lande' factor respectively defined by the following equations.

$$L = \frac{e}{4\pi mc^2} \quad (=4.67 \times 10^{-5}\ cm^{-1}\ gauss^{-1}) \qquad (2)$$

$$g = 1 + \frac{J(J+1) + S(S+1) - L(L+1)}{2J(J+1)} \qquad (3)$$

S, L and J are the quantum numbers of spin, orbital and total angular momentum, respectively.

The intensities of the Zeeman components are expressed as follows.

$$\Delta J = 0 \qquad \begin{array}{ll} \Delta M = 0 & I = 4AM^2 \\ \Delta M = \pm 1 & I = A(J \pm M+1)(J \mp M) \end{array} \qquad (4)$$

$$\Delta J = 1 \qquad \begin{array}{ll} \Delta M = 0 & I = 4B(J+M+1)(J-M+1) \\ \Delta M = \pm 1 & I = B(J \pm M+1)(J \pm M+2) \end{array} \qquad (5)$$

Here, I is the intensity of the transition; A and B are constants.

When $S = 0$, $J(J+1) = L(L+1)$, g becomes 1 and the splitting of the energy levels in a magnetic field are equal and independent of the values of J or L. Therefore, a simple pattern called the normal Zeeman triplet results, as is shown in Figure 1 a). When $S \neq 0$, the splitting of the energy levels depends upon the value of J and L. Then, complicated anomalous Zeeman patterns are observed. Figure 1 b) illustrates the anomalous Zeeman effect of the sodium D lines.

The emission of the π component ($\Delta M = 0$) is linearly polarized in parallel to the magnetic field, while the polarizations of $\sigma^{\pm}$ components ($\Delta M = \pm 1$) are perpendicular to the direction of magnetic field. When the transition is observed in the direction longitudinal to the magnetic field, the σ^{+} component ($\Delta M = 1$) and the σ^{-} component ($\Delta M = -1$) are circularly polarized and the transition of $\Delta M = 0$ is forbidden.

All the Zeeman AA techniques utilize two fundamental phenomena of the Zeeman effect, i.e., the shift and the polarization of atomic lines.

In the case of the polarized Zeeman AA (PZAA) technique, a steady magnetic field is applied to the sample vapor and the difference of absorption is observed between light polarized parallel and perpendicular to the field.

Figure 2 shows the relationship between the profiles of the emission and the absorption line for each observation on the parallel ($P_{//}$) and the perpendicularly ($P_{\perp}$) polarized components of the emission line. This is the case of the Cd resonance line at 228.8 nm = ($^1S_0$-$^1P_1$). These profiles are

obtained from the Voigt function. Although the absorption line is broadened and shifted by the Lorentz and the Doppler effects, only the wavelength of the π component at a suitable magnetic field can be coincident with that of the emission line from the light source. The wavelengths of both the $\sigma^{\pm}$ components are separated completely from the emission line at the same strength of the magnetic field. Therefore, it is evident that the emission line from the field free source can be absorbed by the atomic vapor when its direction of polarization is parallel to the magnetic field but no absorption is observed when the polarization is perpendicular to the field. The intensity of each polarized component of the light beam after absorption can be described as follows:

$$I_{\parallel}(H) = I_{0\parallel} \exp\{-\alpha(n_A K_{\parallel}^{A}(H) + n_B K_{\parallel}^{B}(H))\}, \quad [6]$$

$$I_{\perp}(H) = I_{0\perp} \exp\{-\alpha(n_A K_{\perp}^{A}(H) + n_B K_{\perp}^{B}(H))\}. \quad [7]$$

Here, $K_{//}^{A}(H)$ and $K_{//}^{B}(H)$ are the coefficient of atomic absorption and background absorption for $P_{//}$, respectively. $K_{\perp}^{A}(H)$ and $K_{\perp}^{B}(H)$ are those for $P_{\perp}$, n_A and n_B are the number of atoms and apparent number of background absorbers, α is a constant, and $I_{0//}$ and $I_{0\perp}$ are incident intensities of the $P_{//}$ and $P_{\perp}$, respectively. When the incident light is unpolarized or circularly polarized light, $I_{0//} = I_{0\perp}$. Since the background absorption, the molecular absorption and light scattering are independent of the polarization of incident light, $K_{//}^{B}(H) = K_{\perp}^{B}(H)$. Thus, the following relation is obtained from Eqs. (6) and (7).

$$\log I_{\parallel}(H) - \log I_{\perp}(H) = -\alpha n_A \{K_{\parallel}^{A}(H) - K_{\perp}^{A}(H)\} \propto n_A \qquad [8]$$

Then, we can obtain a signal proportional to n_A, the true number of atoms, without any interference with the background absorption.

Zeeman patterns of the absorption lines used in AAS of various elements are classified to several groups as shown in Figure 3. The principal absorption lines of the elements in the groups IIA and IIB show the spectral pattern (i) (normal triplet). The lines with a notation * are used most frequently for conventional AAS. The structure due to the anomalous Zeeman effect is shown in (ii)-(viii) of Figure 3. The principal doublet of the elements in IA and IB groups show the spectral pattern like (ii) or (iii). Both the spectral patterns like (vi) and (vii) are typical cases of the anomalous Zeeman effect that results from transition between levels of high J values. Group vi is characteristic of transitions between integral J values and group vii between half integral J values.

The absorption lines used for the analysis of the elements in groups VIII, IIIA, IIIB, IVA, VA, VIA, VIB, VIIA and VIIB are classified to these cases. The spectral patterns (iv) and (v) are of the elements belonging to VB. The principal lines of the IVB elements and the secondary lines of the IIB show the spectral patterns of (viii).

Although there are many π and σ components in the case of the anomalous Zeeman effect, the group of the π components are separated from the group of

σ components. Therefore, this technique still has application for lines which show anomalous Zeeman effect. In this case, however, the sensitivity is slightly reduced because the absorption line is broadened.

Figure 4 compares the situation for transitions that show normal Zeeman effect with transitions that show anomalous Zeeman effect. Figure 4 a) shows the observed relationship between the absorption intensities $P_{//}$, $P_{\perp}$ and the magnetic field strength for Zn and Mg which are elements that show normal Zeeman effect. The absorption intensity depends upon the field strength in the case where the radiation from the hollow cathode lamp is polarized perpendicular to the field. But the absorption intensity is independent of the field strength in the case where the radiation from the hollow cathode lamp is polarized parallel to the field.

Figure 4 b) shows the observed relationship between the absorption intensities and the magnetic field strength as for Mn and Ni which are elements that show the anomalous Zeeman effect. In this case, not only the absorption intensity $P_{\perp}$, but also the intensity $P_{//}$ depends upon the field strength. This is true because some of the π components overlap the emission line.

The resonance lines of Hg and Pb have the complicated hyperfine structures, but this causes no problem as is shown in Figure 4 c). These observed relationships between the absorption intensities of $P_{//}$ and $P_{\perp}$ and the field strength show that it is possible to obtain sufficient sensitivity, namely, sufficient difference of absorption, if the suitable strength magnetic field is applied to the sample vapor. Suitable field strength in this case is from 8 to 15 kgauss.

Instrumentation

Figure 5 is the blockdiagram of the polarized Zeeman AA spectrophotometer. Figure 6 shows optics of this instrument. The main part (Figure 7) consists of a rotating linear polarizer, graphite furnace and permanent magnet. The linear polarizer (senarmon prism) is made of artificial quartz blocks with optical contact and can be used over the wavelength range 180 - 1000 nm with a polarization ratio of higher than 99%. It was fixed on a shaft of a synchronous motor that is capable of rotating at 3000 rpm. The polarized beams perpendicular and parallel to the field pass through the graphite cuvette alternately, with rotation of the prism. The difference of absorption is observed between these polarized beams.

Since only a single hollow cathode lamp is used, highly precise background correction is possible for all elements using a simple optical arrangement that does not require tedious alignment procedures. The optical axes of the sample and the reference beams are exactly aligned at all times in this instrument. The light intensity is modulated at 1.5kHz to eliminate blackbody radiation from the furnace.

The synchroscope traces of the signal are shown in Figure 8. The hollow cathode lamp was operated by supplying the modulated current. The modulated light from the lamp with a frequency at 1.5 kHz is absorbed by atomic vapor in the furnace. Since the light intensity is further modulated

at 100 Hz with the rotation of the linear polarizer, the magnitude of the modulation at 100 Hz corresponds to the differential absorption between $P_{//}$ and $P_{\perp}$. The signal from the photomultiplier was amplified by a preamplifier (Figure 8 a), and entered into a mechanical band pass filter. The central frequency and the flat region of the band pass filter were 1.5 kHz and ±110 Hz, respectively. The constituent of the signal with the frequency of 1.39 to 1.61 kHz could pass through the filter (Figure 8 b). The signal was processed to obtain only the 100-Hz component corresponding to the atomic absorption (Figure 8 c and 8 d). The signal due to the blackbody radiation from the graphite cuvette was eliminated by this band pass filter. The 100-Hz component was transformed into logarithm (Figure 8 e), and passed through a line pass filter at 100 Hz, and detected by a synchronous rectifier (Figure 8 f). To improve the precision of logarithm conversion, the high voltage supplied to the photomultiplier was automatically controlled by a feedback loop so that the intensity of the signal due to $P_{\perp}$ was kept at a constant level. The response time of the total system was 0.1 s.

Figure 9 shows the construction of the cup type cuvette placed between the magnet. The absorption region of this cuvette is separated from the atomization region. The sample is atomized in the sample cup, which is at a lower temperature than the absorption cell. The atomized vapor then diffuses in a vertical direction and passes through the absorption cell. The temperature of the absorption cell is higher than that of the bottom of the cup because of differences of heat capacity and electric resistance. However, the temperature of the cup is homogeneous and the rate of vaporization is independent on the position of the sample loaded in the cup. Thus, good reproducibility is obtained without special care in the manner of sample introduction.

Basic Capabilities

This technique has many advantages over conventional AA including those instruments that use various methods of background correction[33)-37)]; namely, the background is precisely corrected at exactly the same wavelength as that of the atomic absorption line; the base line does not change with time even when the radiation intensity does; the double beam optics are optimized because both the sample light and reference light follow exactly the same path through the sample vapor; and, interference caused by direct spectral overlap of absorption lines can be largely eliminated.

In Figure 10, the background correction capability of the Polarized Zeeman AA technique is demonstrated. The correct signal is obtained even when the incident light is attenuated 97.6% (Abs. 1.62) by a fine screen filter. Although the base line noise is slightly increased because the light intensity is decreased, the base line does not shift.

The worst possible case of molecular absorption may be that of nitric oxide (NO) interference in the determination of Zn because one of the rotation lines of NO is very close (0.86 cm^{-1}) to the Zn analytical line at 213.8 nm [38)]. Even in this case, the strong molecular absorption caused by a mixture of NO and NO_2 (absorbence 2.3 of transmittance 0.5%) did not give rise to a detectable interference signal with the PZAA technique as shown in Figure 11. The only effect was an increase in noise level because of the strong attenuation of the incident light. Almost any conceivable case of molecular absorption interference can be corrected by this technique.

Figure 12 shows a comparison between the base line variation obtained with the present instrument and with a conventional atomic absorption spectrophotometer. These base lines were recorded just after lighting the hollow cathode lamp. The base line of the conventional atomic absorption spectrophotometer drifts with time, but base line of the PZAA instrument is very stable and shows very little drift with time. This improvement results because this technique provides double beam cor ections by using the $P_{\perp}$ as a reference and $P_{//}$ as a sample beam.

In addition to the precise background correction, interference caused by direct spectral overlap between absorption lines can be corrected by this technique [24].

Interference by direct spectral overlap occurs if another element is capable of absorbing radiation meant for the analyte. This kind of spectral interference brings about serious errors in atomic absorption spectrometry. An apparent signal is obtained even when the analyte is not present in the sample. This type of interference cannot be eliminated by using a smaller spectral band pass or the standard addition method. On more than 10 lines, interference due to direct spectral overlap was reported and about 50 cases of potential spectral overlap within 0.03 nm were found in an Atlas of Spectral lines.

This kind of interference can be corrected by the PZAA technique because the absorption intensities of the π and $\sigma^+ + \sigma^-$ components are almost the same in the wings of the interfering absorption line.

The profile of the wings of an absorption line is expressed by the following equation [32].

$$\kappa(\nu) \propto |\nu - \nu_0|^{-\delta} \qquad \delta = \begin{cases} \frac{5}{4} & \text{(blue wing)} \\ \frac{3}{2} & \text{(red wing)} \end{cases} \tag{9}$$

Here, $\kappa(\nu)$ = absorption coefficient at a frequency ν, ν = frequency of the light, ν_0 = frequency of the line center. When the sample vapor is placed in a magnetic field, the interfering absorption line splits into π and σ Zeeman components, which absorb the polarized radiation $P_{//}$ and $P_{\perp}$ respectively.

Then, when the emission line lies at a frequency in the wing of this absorption line, the ratio of the absorption intensity of $P_{//}$ and $P_{\perp}$ is expressed by the following equation in the case of a simple Zeeman triplet pattern.

$$\frac{\kappa_\pi}{\kappa_\sigma} = \frac{|\nu-\nu_0|^{-\delta}}{\frac{1}{2}|\nu-\nu_0+\Delta\nu_z|^{-\delta}+\frac{1}{2}|\nu-\nu_0-\Delta\nu_z|^{-\delta}} \tag{10}$$

Here, $\Delta\nu_z$ = Zeeman shift of the absorption line, κ_π, κ_σ = absorption coefficients of π and σ components at frequency ν, respectively.

If $\nu-\nu_0 < \Delta\nu_z$, $\frac{\kappa_\pi}{\kappa_\sigma}$ becomes 1. This means $\kappa^{A}(H) - \kappa^{A}(H)$ in Eq. (8) becomes 0. Therefore, no interference signal occurs because the difference

of absorption between $P_{//}$ and $P_{\perp}$ is observed in the Polarized Zeeman AA technique.

Figure 13 shows the comparison of direct line overlap interference between conventional AA and this technique. Figure 13 a) shows the observed spectral interference of Sb with Pb in conventional atomic absorption. The Sb hollow cathode lamp was set in the conventional AA spectrophotometer, and the wavelength was adjusted so as to peak light intensity around 217.5 nm. Widths were 0.8 and 1.0 nm for the entrance and the exit slits, respectively, and the resolving power was 2.25 nm. Standard solutions of Pb of 10 µl were atomized by utilizing the graphite atomizer at 2000°C. D_2 lamp correction was employed to eliminate the interference of background absorption. Although Sb was absent in the Pb standard solutions, the radiation from the Sb hollow cathode lamp was clearly absorbed as shown in Figure 13 a). Figure 13 a) shows that only a few ppm of Pb in a sample brings about a serious error in the analysis for Sb.

Figure 13 b) shows that this kind of spectral interference can be eliminated by the Polarized Zeeman AA technique, even the high concentration Pb standard solution of 1000 ppm did not give a rise to an absorption signal. A 0.5 ppm Sb solution shows an absorbence of 0.05 under these conditions. The monochromator and the slit width in the Polarized Zeeman AA spectrophotometer were exactly the same as those used in the conventional AA spectrophotometer and also a similar type of graphite furnace atomizer was used in both instruments. Therefore, we can say that the difference between Figures 13 a) and Figure 13 b) is totally caused by the difference between Polarized Zeeman AA and conventional AA spectroscopy.

Figure 14 demonstrates the high sensitivity of this technique. This figure shows the large absorption signals obtained with very low concentration Cd and Pb solution (1 ppb). 100 µl of lead solution was introduced into the cup type cuvette by repeating the drying five times. The upper limit of the linear range of the detection depends upon the absorption lines of the elements. For example, calibration curves of Ag and Cr are linear up to higher than 1.0 and 0.5 absorbence units (defined as the difference in absorption between $P_{//}$ and $P_{\perp}$). However, Cd and Zn have a comparatively small dynamic range (up to abs. 0.25 at the magnetic field at 11 kgauss) because the apparent saturation of absorption of $P_{//}$ by the π components comes faster than that of $P_{\perp}$ by the wing of the $\sigma^{\pm}$ components. However, it is easy to measure samples of comparatively high concentration by reducing the sensitivity from 1/5 to 1/15 by increasing the carrier gas flow.

Table 2 shows the lower limits of detection for various elements, the wavelength of the light used for the observation, and the relevant electronic states. High sensitivity is obtained by this technique even for transitions which show the complicated anomalous Zeeman patterns, or that have large hyperfine structure. This Figure also lists an example of the detection limit obtained by a conventional atomic absorption spectrophotometer with a similar type of a graphite furnace atomizer. For example, Co and Cr show the complicated Zeeman patterns, but the detection limits are almost the same as those obtained by the conventional method without the background correction. Unlike the conventional atomic absorption spectrophotometer, the detection limits of the Polarized Zeeman instrument were measured by

employing both the background correction and the double beam optics. Thus we see the same order of detection limit is obtained along with the advantages of stable base line and superior background correction ability.

Applications of Zeeman AA Technique

1) Highly reliable analysis of samples of unknown matrix [39]

In the quantitative determination of trace elements, it is very important to develop techniques which will result in an accurate analysis when the sample is of unknown composition. This is especially true when the number of samples is so large and varied that it is difficult to keep detailed records. The standard addition method has been used as an empirical technique to reduce analytical errors for some systems. However, standard addition can correct multiplicative type errors brought about by chemical interference, but it does not correct an additive type of interference which gives an additive factor to the calibration curve. With the Polarized Zeeman AA technique, all of the interferences which cause the additive interference factor to be nonzero can be eliminated. Therefore, the analytical result is highly reliable, even though the sample matrix may be complex, when the standard addition method is used with this technique.

Table 3 shows the result of the determination of several elements in SRM-1643 (Trace Elements in Water). Good agreement was obtained between

the results by the Polarized Zeeman AA technique and the other techniques. The precision of the PZAA measurement was better than 3% in coefficient of variables.

The composition of SRM-1643 is close to that of natural water; major constituents are Ca 27 μg/g, Na 10 μg/g, Mg 7 μg/g and K 2 μg/g. Nitric acid is present at a concentration of 0.5 N to stabilize the trace elements.

This sample was then mixed with a high concentration salt solution and the trace elements were determined once more. The direct analysis of trace elements in such a highly concentrated salt solution is impossible with conventional AA. Figure 15 shows standard addition curves for the determination of Ag in SRM-1643. Curves (1) and (2) were obtained from an unaltered sample of SRM-1643 and a mixture of SRM-1643 and 20,000 ppm of NaCl, respectively. NaCl cannot be eliminated by an ashing process because its vaporization temperature is higher than that of Ag.

The large quantity of NaCl causes strong molecular absorption and light scattering. However, any additive factor is not observed, since the Polarized Zeeman AA technique especially corrects for these types of interference. Even though the concentration of the interferent was about 6×10^6 times larger than the analyte atom, an accurate result was obtained with this technique.

2) Analysis of high salinity sample

Various kinds of salts such as NaCl and KCl have strong absorption

bands in U.V. region and cause very strong background absorption. Therefore, with conventional AA it is very difficult to directly analyze the trace elements in samples of sea water or river water near the point where it merges with the ocean. However, direct analysis of sea water is possible with polarized Zeeman AA. Figure 16 shows the direct determination of Cd in natural sea water. Figure 17 demonstrates the high accuracy of a determination of this kind. First Cd was determined in a sample of simple matrix using the standard addition method. Next it was mixed with sea water and Cd was determined once again. The calibration curves for both samples cut the same point on the concentration axis, as shown in Figure 17. Background levels of trace elements in unpolluted sea water are extremely low and, with a few exceptions, cannot be detected even though the PZAA technique is utilized. However, if some area of the sea or river was subject to metal pollution, the contamination could be detected. This technique is also applicable to the analysis of high salinity wastewater from industry.

3) Clinical Analysis

This technique is also applicable to the determination of trace elements in blood, serum and urine with minimum sample preparation. Figure 18 shows the results of the determination of Cu in serum. A standard solution of Cu was added to the serum to provide samples of an additional 1.0, 0.5 and 0 ppm of Cu. No ashing process was employed in this measurement. The small peak or fluctuation of the base line is due

to the surface reflection of bubbles of serum which is formed during the drying process. The measured Cu concentration in the original serum was 0.89 ppm.

4) Steel Analysis

Various kinds of interference by the major constituents make it difficult to directly determine the trace elements in a steel or alloy sample with conventional AA. Background correction is necessary to eliminate the scattering and the molecular absorption from the compounds formed by the major constituents. However, background correction by a continuum source brings a different kind of interference caused by major constituents that have numerous absorption lines like Fe, Ni, Co. A number of absorption lines falling in the band pass of a monochromator often give rise to over-estimation of the background absorption. Only the reference beam from a continuum source is absorbed by the large concentration of Fe, Ni, and Co atoms. Figure 19 shows the typical interference in conventional AA for the analysis of Sb in a Ni matrix. In this case, the radiation from the D_2 lamp was more strongly absorbed by Ni atoms than the radiation from the Sb hollow cathode lamp. This is because many absorption lines of Ni around 231 nm including the sensitive at 231.096 nm line fall within the band pass of the monochromator and absorb the continuum from the D_2 lamp, while the Sb radiation at 231.147 nm is slightly absorbed by only the wing of the Ni line at 231.096 nm.

The same type of interference for other elements is frequently

observed in steel analysis. Because of interference of this kind, conventional AA instruments are difficult to use for the determination of trace elements in steel.

With polarized Zeeman AA, over-estimation of the background absorption does not occur. Figure 20 shows that both the effect of over-correction and direct spectral overlap are eliminated. An example of the analysis of a Standard Steel Sample using PZAA is shown in Table 4.

5) Analysis of gun powder residue

Several different elements (i.e., Sb, Ba) are determined in gun powder residue for forensic purposes. The gun powder residue is collected from the hands of the suspect using a wet swab. When the sample is taken from dirty hands, contamination often causes a problem. We observed high levels of Pb, Zn, Ca, Na and, if the suspect had handled coins, Ni, Cu and Ag from these samples. In conventional AA, the Pb and Ni contamination give rise to the direct spectral line overlap interference in the determination of Sb.

Sb lines at 217.023 nm and 231.147 nm overlap the Pb absorption line at 216.999 nm and the Ni absorption line at 231.096 nm respectively. Both interferences from furnace emission and background absorption by CaO have to be eliminated in the determination of Ba.

The PZAA spectrophotometer is free from all of these interferences. Figure 21 shows an example of gun powder residue analysis. The sample from

the right hand contains Sb, but the sample from the left hand does not. This means that the gun was fired with the right hand.

6) Speciation of organometallic compounds with HPLC

Species determinations by the determination of atomic constituents have application to the field of biochemistry because many enzymes and coenzymes have a metal atom in their functional center. Speciation is also important in the environmental field because the toxicity of a metal depends upon its chemical form. ZAA is a valuable new technique for organometallic species determination by interfacing with a high pressure liquid chromatograph (HPLC) because of its high selectivity and high sensitivity. The HPLC separates various molecular species. Different kinds of mobile solvents can be directly introduced in the ZAA detection system; even organic solvents or high concentration salt solutions. Using this detection method, organometallic species in the ppb range can be separately detected according to their retention times.

A demonstration of the operation of this system is provided by the analysis of a mixture of Vitamin B12 and $Co(NO_3)_2$ [40]. As shown in Figure 22, Vitamin B12 has a Co in its functional center. Sample 1 contained Co at a concentration of 0.813 µg/ml that was present in Vitamin B12 (cyanocobalamine form) and Co at a concentration of 25.0 µg/ml that was introduced as $Co(NO_3)_2$. Sample 2 contained only Vitamin B12 at the same concentration as that in Sample 1. 0.5 ml of the sample was eluted with CH_3COONH_4 [2 M] through an anion exchange column at a flow rate of 1.0 ml/min, and pressure of 20 kg/cm^2.

The separation between Vitamin B12 and $Co(NO_3)_2$ was confirmed by using U.V. absorption and coulometry[11] simultaneously. The upper and lower traces in Figure 22 show the signals from the coulometric detector and the U.V. absorption detector, respectively. The first peak in the lower trace shows the appearance of the Vitamin B12 and the second peak in the upper trace, the appearance of the $Co(NO_3)_2$.

Next, fractions A, B and C with retention times between 2-5, 5-8, 8-11 min., respectively, were collected for both Sample 1 and Sample 2. 10 µl from each fraction of 3 ml was introduced into the ZAA spectrophotometer and the concentration of Co was measured at the wavelength of 240.7 nm. Figure 23 shows the absorption signal of Co for each fraction. Figure 23 a) shows that the concentration of Co bound to Vitamin B12 could be obtained without interference even though the coexisting inorganic Co concentration was 30 times larger than that of Co in Vitamin B12.

Figure 23 b) shows that the concentration of the inorganic Co could be obtained separately from the Co in Vitamin B12.

Recently we developed a new type of furnace which can effectively atomize organometallic compounds without drying and ashing. By utilizing this furnace for the ZAA-HPLC system, we performed the species determination of alkyl lead compounds in NBS gasoline standards. This work will soon be published in Analytical Chemistry [41].

Acknowledgments

The author thanks T. Hadeishi and R. D. McLaughlin of Lawrence Berkeley Laboratory of the University of California, S. Hanamura and L. L. Barnes of National Bureau of Standards, and J. D. Westhoff of Environmental Effect Laboratory of U.S.A.E. Water Ways Experimental station for their helpful suggestions.

The author also thanks K. Yamada of Naka Works, Hitachi Ltd. for the analysis of the steel sample with this technique.

Work supported by the U. S. Department of Energy.

References

* Guest Researcher at Lawrence Berkeley Laboratory in 1977-1978
Permanent address: Naka Works, Hitachi Ltd., Katsuta, Ibaraki 312, Japan

1. P. Zeeman, Philosophical Magazine, 43, 226 (1897)

2. E. U. Condon and G. H. Shortrey, The Theory of Atomic Spectra, Cambridge University Press, London (1935)

3. S. Mrozowski, Nature, 127, 890 (1930)

4. J. Brossel and F. Bitter, Phys. Rev. 86, 308 (1952)

5. T. Hadeishi and R. D. McLaughlin, Science, 174, 404 (1971)

6. T. Hadeishi, Appl. Phys. Lett., 21, 438 (1972)

7. D. A. Church, T. Hadeishi, L. Leong, R. D. McLaughlin and B. D. Zak, Anal. Chem., 46, 1352 (1974)

8. T. Hadeishi, D. A. Church, R. D. McLaughlin, B. D. Zak, M. Nakamura and B. Chang, Science, 187, 348 (1975)

9. H. Koizumi and K. Uchino, Hitachi Hyoron, 56, 1037 (1974); Chem. Abstr., 83, 21386J

10. H. Koizumi and K. Yasuda, Anal. Chem., 47, 1679 (1975)

11. R. Stephens and D. E. Ryan, Talanta, 22, 655 (1975)

12. R. Stephens and D. E. Ryan, Talanta, 22, 659 (1975)

13. H. Koizumi and K. Yasuda, Spectrochim. Acta, 31B, 237 (1976)

14. T. Hadeishi and R. D. McLaughlin, Anal. Chem., 48, 1009 (1976)

15. H. Koizumi and K. Yasuda, Anal. Chem., 48, 1178 (1976)

16. D. E. Veinot and R. Stephens, Talanta, 23, 849 (1976)

17. R. Stephens, Talanta, 24, 233 (1977)

18. T. Hadeishi and T. Andersen, Opt. Com. 23, 252 (1977)

19. J. C. Robbins, Geochemical Exploration, P 315 (1972)

20. H. Koizumi and K. Yasuda, Spectrochim. Acta, 31B, 423 (1976)

21. J. B. Dawson, E. Grassam, D. J. Ellis and M. J. Keir, Analyst, 101, 315 (1976)

22. H. Koizumi, K. Yasuda and M. Katayama, Anal. Chem., 49, 1106 (1977)

23. E. Grassam, J. B. Dawson and D. J. Ellis, Analyst, 102, 804 (1977)

24. H. Koizumi, Anal. Chem., 50 (1978)

25. Y. Uchida and S. Hattori, Oyo Butsuri, 44, 852 (1975); Chem. Abstr. 84, 11953Y.

26. A. Ballard, D. W. Stewart, W. O. Kamm, C. W. Znehlke, Anal. Chem., 26, 921, (1954)

27. A. Walsh, Spectrochim. Acta. 7, 108 (1955)

28. S. D. Brown, Anal. Chem., 49, 1269A (1977)

29. G. M. Hieftje and T. R. Copeland, Anal. Chem., 50, 300R (1978)

30. M. Katayama and H. Koizumi, Chem. Today, 69 (12), 34 (1976), 70 (1), 36 (1977)

31. R. J. Lovett, D. L. Welch and M. L. Parsons, Appl. Spectrosc. 29, 470 (1975)

32. H. Kuhn, Proc. R. Soc., A, 158, 212 (1937)

33. W. Slavin, At. Absorption Newsl. 24, 15 (1964)

34. S. R. Koirtyohann and E. E. Pickett, Anal. Chem. 37, 601 (1965)

35. J. Kuhl, G. Marowsky and R. Torge, Anal. Chem, 44, 375 (1972)

36. C. Ling, Anal. Chem, 39, 798 (1967)

37. C. Ling, ibid, 40, 1876 (1968)

38. L. A. Melton and W. Klemperer, J. Chem. Phys., 59, 1099 (1973)

39. H. Koizumi, S. Hanamura and I. L. Barnes, to be published

40. H. Koizumi, T. Hadeishi and R. D. McLaughlin, Lawrence Berkeley Laboratory Report, LBL-6993 (1978)

41. H. Koizumi, R. D. McLaughlin and T. Hadeishi, to be published

Figure Captions

Figure 1 Comparison of normal and anomalous Zeeman effect.

Figure 2 Relationship between the emission and the absorption line for the situation when the direction of polarization of the emission line is parallel and perpendicular to the magnetic field; direction of the observation is perpendicular to the magnetic field applied to the sample vapor (Cd line at 228.8 nm, magnetic field at 10 kgauss).

Figure 3 Classification of Zeeman patterns of various elements.

Figure 4 (a) Relationship between the absorption intensities and of light polarized parallel to the magnetic field ($P_{//}$), light polarized perpendicular to the magnetic field ($P_{\perp}$) and the magnetic field strength for Zn and Mg. (b) Relationship between the absorption intensities $P_{//}$, $P_{\perp}$ and the magnetic field strength for Mn and Ni. (c) Relationship between the absorption intensities $P_{//}$, $P_{\perp}$ and the magnetic field strength for Hg and Pb.

Figure 5 Block diagram of the polarized Zeeman atomic absorption spectrophotometer.

Figure 6 Optics of polarized Zeeman AA instrument.

Figure 7 Main part of polarized Zeeman AA spectrophotometer.

Figure 8 Oscilloscope display of each stage of the signal processing.

Figure 9 Cross-section of cup type cuvette.

Figure 10 Precision of background correction with PZAA technique.

Figure 11 Correction of the sharp and strong background absorption caused by No and NO_2 mixture with PZAA technique.

Figure 12 Comparison of baseline drift of a conventional single beam atomic absorption spectrophotometer with the polarized Zeeman AA instrument.

Figure 13 (a) Observed interference by Pb in the determination of conventional AA spectrometry. (wavelength: 217 nm, light source: Sb).
(b) Elimination of spectral interference caused by Pb in the determination of Sb in the polarized Zeeman AA technique (wavelength: 217 nm, light source: Sb).

Figure 14 Signals from low concentrations of Pb and Cd (1 ppb) using the PZAA technique.

Figure 15 Standard addition curves that result from the determination of Ag in the NBS standard reference material SRM-1643, and a 1:1 mixture of SRM-1643 and NaCl 20,000 ppm obtained with PZAA. (The same result is obtained from both the samples).

Figure 16 Direct determination of Cd in natural sea water.

Figure 17 Determination of Cd in a sample and 1:1 mixture of the sample and sea water by PZAA. (The same result is obtained from both the samples).

Figure 18 Direct determination of Cu in serum.

Figure 19 Interference caused by Ni when conventional AA with D_2 lamp background correction is used. (wavelength: 231 nm, light source: Sb and D_2 lamps).

Figure 20 Elimination of spectral interference caused by Ni in the determination of Sb using the PZAA technique. (wavelength: 231 nm, light source: Sb).

Figure 21 Detection of Sb in gun powder residue from hands.

Figure 22 Separation between Vitamin B12 and $Co(NO_3)_2$ by HPLC. Upper trace: coulometric detector, Lower trace: U. V. absorption detector.

Figure 23 Detection of Co from fraction A, B and C.

Table 1. Zeeman Atomic Absorption Spectroscopy

Emission Line Shifted Zeeman AA	⎡	Isotope Zeeman AA (IZAA) [5)-8)]
	⎢	π, σ Zeeman AA (ZAA) [9)-18)]
	⎣	Field Modulation Zeeman AA [19)]
Absorption Line Shifted Zeeman AA	⎡	Polarized Zeeman AA (PZAA) [20)-24)]
	⎣	Field Modulation Zeeman AA [25)]

Table 2 Detection limits of various elements
(the quantities of metal at s/n=2, magnetic field; 11 kgauss)

Element	Wavelength (nm)	Transition	Present Method	Conventional Method (without background correction)
			Detection Limit (g)	
Ag	328.0	$^2S_{1/2}-^2P_{3/2}$	$9\cdot10^{-13}$	$5\cdot10^{-13}$
Al	309.2	$^2P_{3/2}-^2D_{5/2}$	$2\cdot10^{-11}$	$5\cdot10^{-12}$
Am	193.6	$^4S_{3/2}-^4P_{3/2}$	$1\cdot10^{-11}$	$1\cdot10^{-11}$
Ba	553.5	$^1S_0-^1P_1$	$8\cdot10^{-11}$	$1\cdot10^{-10}$
Bi	306.7	$^4S_{3/2}-^4P_{1/2}$	$3\cdot10^{-11}$	$1\cdot10^{-11}$
Ca	422.6	$^1S_0-^1P_1$	$4\cdot10^{-12}$	
Cd	228.8	$^1S_0-^1P_1$	$3\cdot10^{-13}$	$3\cdot10^{-13}$
Co	240.7	$^4F_{9/2}-^4G_{11/2}$	$2\cdot10^{-11}$	$4\cdot10^{-11}$
Cr	359.3	$^7S_3-^7P_3$	$9\cdot10^{-12}$	$1\cdot10^{-11}$
Cs	852.1	$^2S_{1/2}-^2P_{3/2}$	$3\cdot10^{-11}$	
Cu	324.7	$^2S_{1/2}-^2P_{3/2}$	$1\cdot10^{-11}$	$5\cdot10^{-12}$
Fe	248.3	$^5D_4-^5F_5$	$4\cdot10^{-12}$	$2\cdot10^{-12}$
Hg	253.6	$^1S_0-^3P_1$	$1\cdot10^{-10}$	
K	766.4	$^2S_{1/2}-^2P_{3/2}$	$2\cdot10^{-11}$	
Li	670.7	$^2S_{1/2}-^2P_{3/2}$	$2\cdot10^{-11}$	$3\cdot10^{-11}$
Mg	285.2	$^1S_0-^1P_1$	$1\cdot10^{-13}$	
Mn	279.8	$^6S_{5/2}-^6P_{5/2}$	$3\cdot10^{-12}$	$1\cdot10^{-12}$
Na	588.9	$^2S_{1/2}-^2P_{3/2}$	$2\cdot10^{-12}$	
Ni	232.0	$^3F_4-^3G_5$	$3\cdot10^{-11}$	$1\cdot10^{-10}$
Pb	288.3	$^3P_0-^3P_1$	$4\cdot10^{-12}$	$5\cdot10^{-12}$
Sb	217.5	$^4S_{3/2}-^4P_{3/2}$	$3\cdot10^{-10}$	$2\cdot10^{-11}$
Sc	196.0	$^3F_2-^3S_1$	$1\cdot10^{-9}$	$5\cdot10^{-11}$
Sr	460.7	$^1S_0-^1P_1$	$2\cdot10^{-11}$	
Ti	319.2	$^3F_3-^3G_4$	$4\cdot10^{-9}$	$2\cdot10^{-9}$
V	318.4	$^4F_{7/2}-^4G_{9/2}$	$4\cdot10^{-10}$	$5\cdot10^{-10}$
Zn	213.8	$^1S_0-^1P_1$	$1\cdot10^{-13}$	$1\cdot10^{-13}$

Table 3 . Comparison of the analytical results obtained by Polarized Zeeman AA and other techniques.(ng/g)

Element	Polarized Zeeman AA	Other techniques
Ag	3.52	3.53 (NA)
Al	76.8	77 (P) 76 (AA)
As	78.5	76.6 (AA)
Pb	20.6	20.04 (TID)
Zn	63.9	64 (P) 63 (NA) 64 (SID)

NA : Neutron activation
P : Polarography
AA : Atomic absorption spectrometry
TID: Thermal source isotope dilution mass spectroscopy
SID: Spark source isotope dilution mass spectroscopy

Table 4. Analysis of Standard Steel

Element	Recommended value, (%)	Result with PZAA, (%)
Co	0.020	0.019 ±0.001
Pb	0.002	0.0017 ±0.00009
Mn	0.10	0.103 ±0.005
Cu	0.044	0.039 ±0.002
Ni	0.019	0.019 ±0.001
Cr	0.014	0.0114 ±0.0006
Sn	0.014	0.0136 ±0.0007
Al	0.006	0.0058 ±0.0003
V	0.10	0.092 ±0.005
Si	0.016	0.02 ±0.001

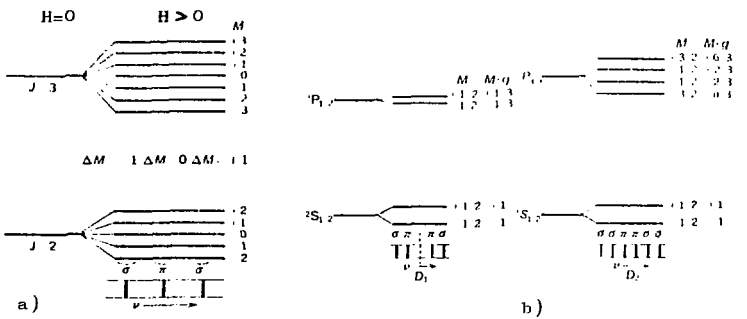
H=0
H > 0
M
J 3
ΔM 1 ΔM 0 ΔM -1
J 2
σ⁻ π σ⁺
a)
b)

Fig.1

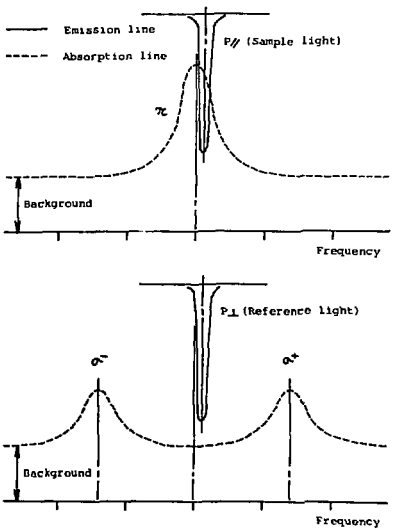
Emission line
Absorption line
P// (Sample light)
π
Background
Frequency
P⊥ (Reference light)
σ⁻
σ⁺
Background
Frequency

Fig.2

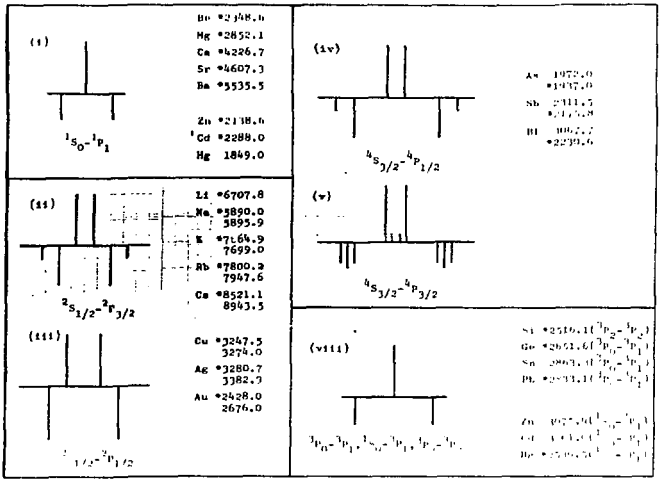
(i)
$^1S_0$-$^1P_1$
Be *2348.6
Hg *2852.1
Ca *4226.7
Sr *4607.3
Ba *5535.5
Zn *2138.6
Cd *2288.0
Hg 1849.0
(ii)
$^2S_{1/2}$-$^2P_{3/2}$
Li *6707.8
Na *5890.0
5895.9
K *7664.9
7699.0
Rb *7800.2
7947.6
Cs *8521.1
8943.5
(iii)
$^2S_{1/2}$-$^2P_{1/2}$
Cu *3247.5
3274.0
Ag *3280.7
3382.9
Au *2428.0
2676.0
(iv)
$^4S_{3/2}$-$^4P_{1/2}$
As *1972.0
*1937.0
Sb *2311.5
*2175.8
Bi *2023.7
*2399.6
(v)
$^4S_{3/2}$-$^4P_{3/2}$
(vi)
$^3F_4$-$^3G_5$
Si *2420.6
Zr *3601.2
Similar Patterns
Al *3092.7($^2P_{1/2}$-$^2D_{5/2}$)(5)
Co *2407.3($^4F_{9/2}$-$^6D_{11/2}$)(10)
Cr 3593.5($^7S_3$-$^7P_3$)(6)
Fe *2483.3($^5D_4$-$^5F_5$)(9)
Mn 2798.3($^6S_{5/2}$-$^6P_{5/2}$)(6)
Mo 3170.4($^7S_3$-$^7P_4$)(6)
Rh *3434.9($^4F_{9/2}$-$^4G_{11/2}$)(10)
V *3184.0($^4F_{7/2}$-$^4G_{9/2}$)(8)
Ru *3498.9($^5F_5$-$^5G_6$)(11)
Y. *4102.4($^2D_{5/2}$-$^2F_{7/2}$)(6)
Zr *3601.2($^3F_4$-$^3G_5$)(9)
(vii)
$^6S_{5/2}$-$^6P_{7/2}$
Mn *2794.8
Similar Patterns
Cr *3578.7($^7S_3$-$^7P_4$)(7)
Mo *3132.6($^7S_3$-$^7P_4$)(7)
Se *1960.3($^3P_2$-$^3S_1$)(3)
Te *2142.8($^3P_2$-$^3S_1$)(3)
( ): Number of fine lines of the component

Fig.3

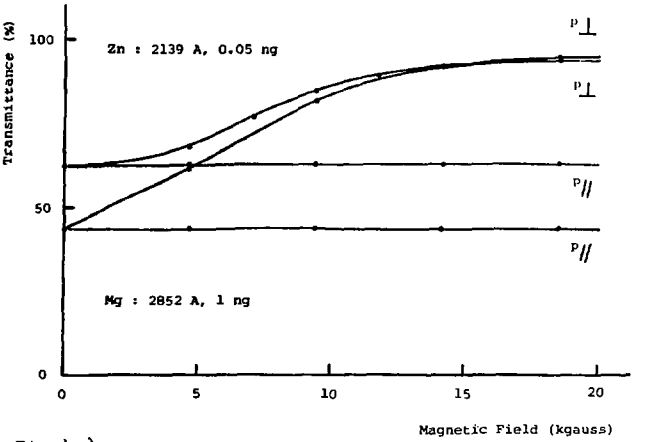
Transmittance (%)
100
50
0
Zn : 2139 A, 0.05 ng
Mg : 2852 A, 1 ng
P⊥
P⊥
P//
P//
0
5
10
15
20
Magnetic Field (kgauss)

Fig.4a)

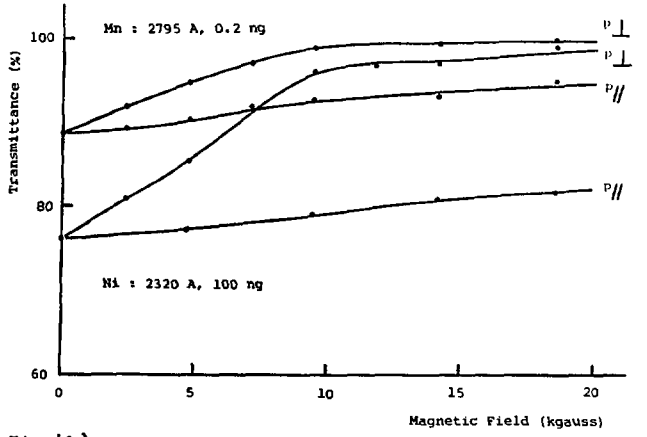
Transmittance (%)
100
80
60
Mn : 2795 A, 0.2 ng
Ni : 2320 A, 100 ng
P⊥
P⊥
P//
P//
0
5
10
15
20
Magnetic Field (kgauss)

Fig.4b)

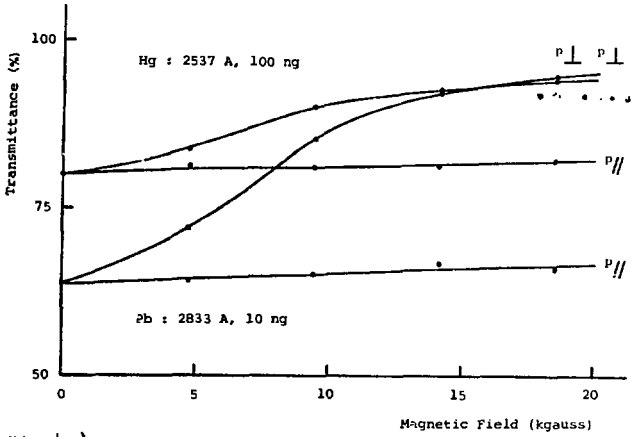
100
75
50
Transmittance (%)
Hg : 2537 A, 100 ng
P⊥ P⊥
P//
P//
Pb : 2833 A, 10 ng
0
5
10
15
20
Magnetic Field (kgauss)

Fig.4c)

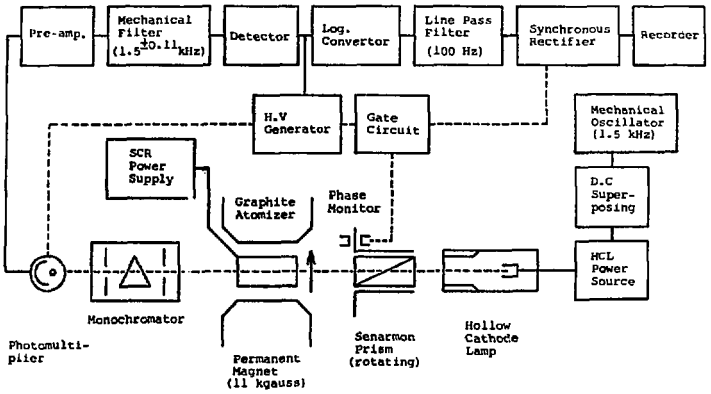
Pre-amp.
Mechanical Filter (1.5 ±0.11 kHz)
Detector
Log. Convertor
Line Pass Filter (100 Hz)
Synchronous Rectifier
Recorder
H.V Generator
Gate Circuit
Mechanical Oscillator (1.5 kHz)
SCR Power Supply
Graphite Atomizer
Phase Monitor
D.C Super-posing
HCL Power Source
Monochromator
Photomulti-plier
Permanent Magnet (11 kgauss)
Senarmon Prism (rotating)
Hollow Cathode Lamp

Fig.5

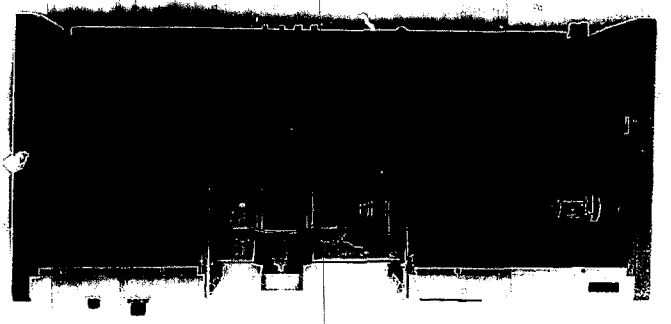

Fig.6

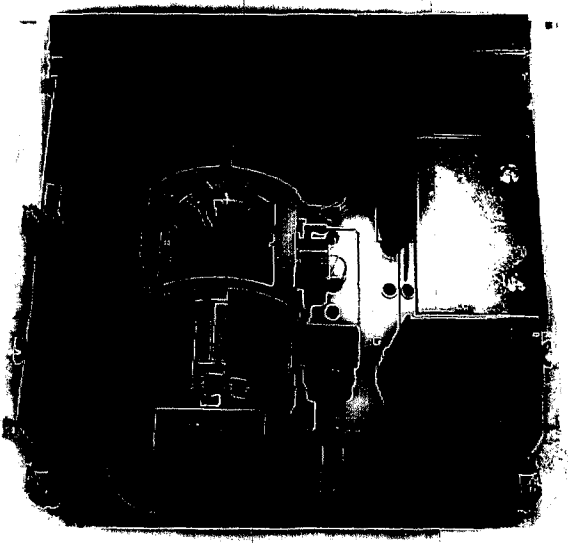

Fig.7

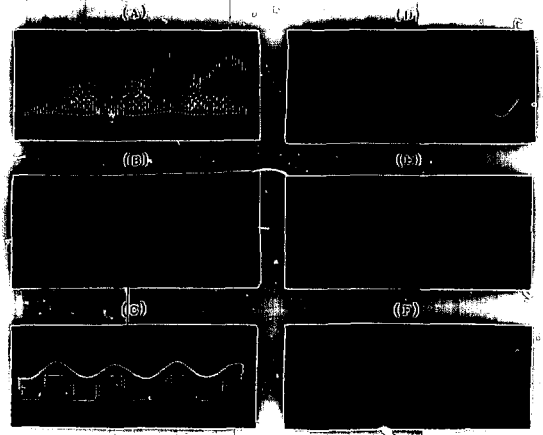

Fig.8

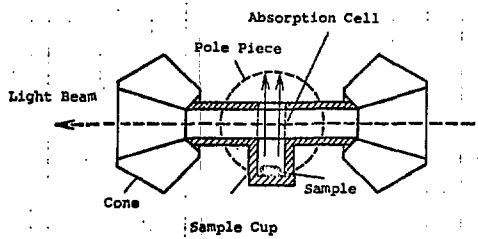
Absorption Cell
Pole Piece
Light Beam
Sample
Cone
Sample Cup

Fig.9

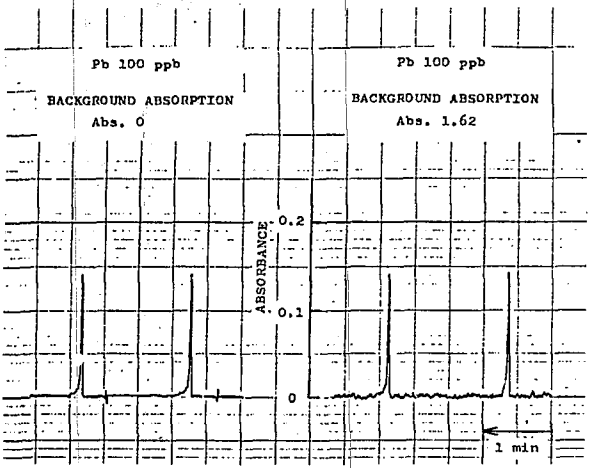
Pb 100 ppb
BACKGROUND ABSORPTION
Abs. 0
Pb 100 ppb
BACKGROUND ABSORPTION
Abs. 1.62
ABSORBANCE
0.2
0.1
0
1 min

Fig.10

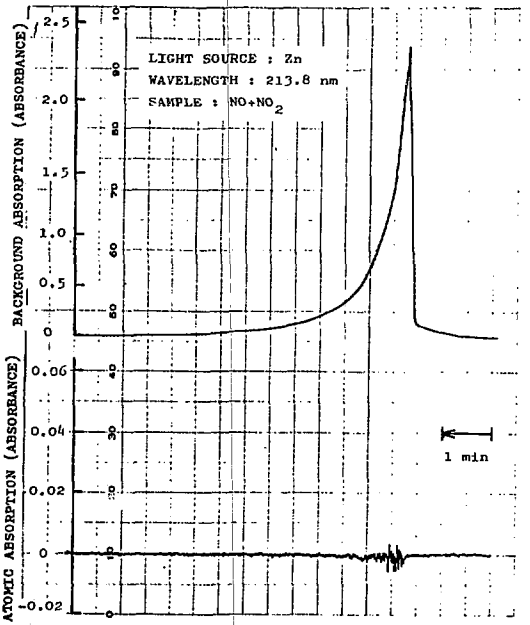
LIGHT SOURCE : Zn
WAVELENGTH : 213.8 nm
SAMPLE : NO+NO2
BACKGROUND ABSORPTION (ABSORBANCE)
2.5
2.0
1.5
1.0
0.5
0
ATOMIC ABSORPTION (ABSORBANCE)
0.06
0.04
0.02
0
-0.02
1 min

Fig.11

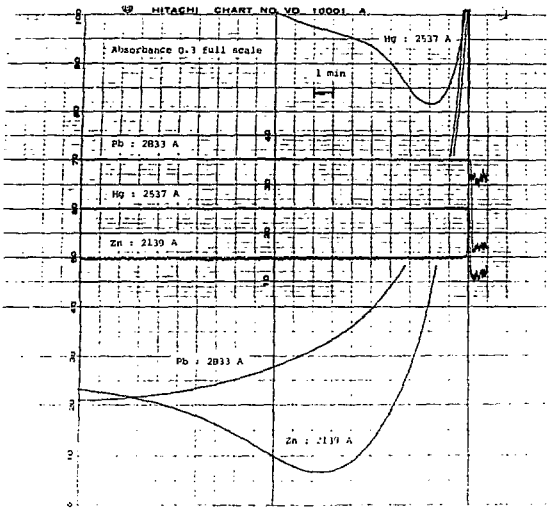
HITACHI CHART NO. VD 10001 A
Absorbance 0.3 full scale
1 min
Hg : 2537 A
Pb : 2833 A
Hg : 2537 A
Zn : 2139 A
Pb : 2833 A
Zn : 2139 A

Fig.12

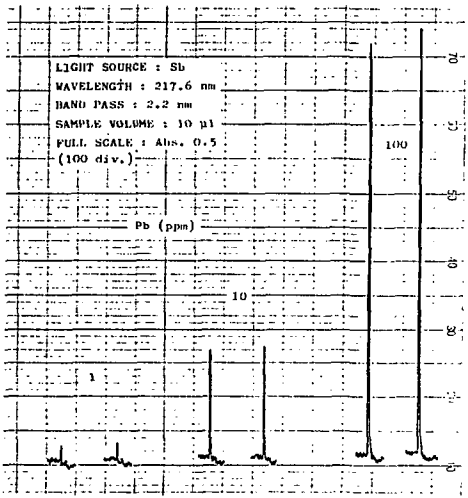

Fig.13a)

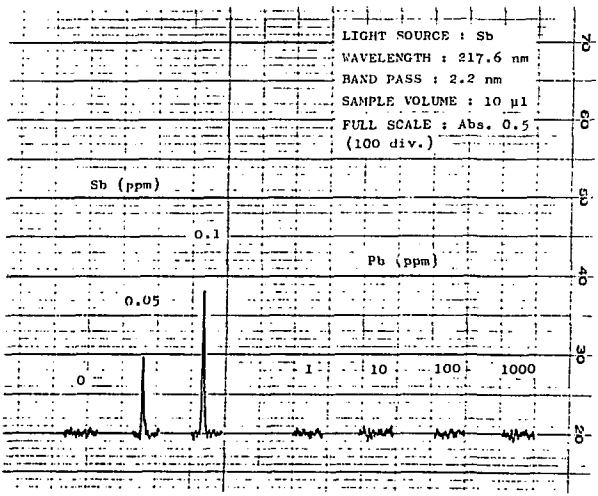

Fig.13b)

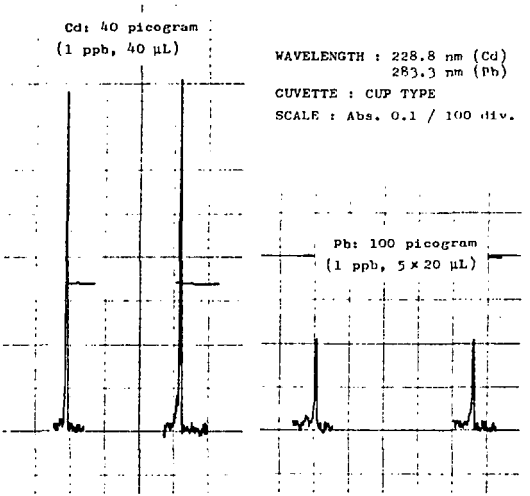
Cd: 40 picogram
(1 ppb, 40 µL)
WAVELENGTH : 228.8 nm (Cd)
283.3 nm (Pb)
CUVETTE : CUP TYPE
SCALE : Abs. 0.1 / 100 div.
Pb: 100 picogram
(1 ppb, 5 × 20 µL)

Fig. 14

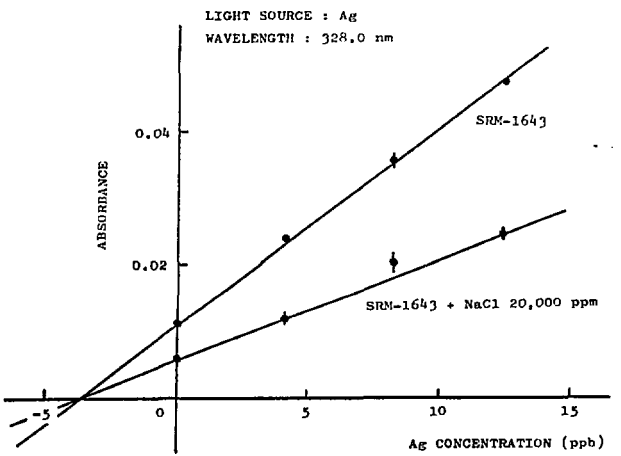
LIGHT SOURCE : Ag
WAVELENGTH : 328.0 nm
SRM-1643
SRM-1643 + NaCl 20,000 ppm
ABSORBANCE
0.04
0.02
-5
0
5
10
15
Ag CONCENTRATION (ppb)

Fig.15

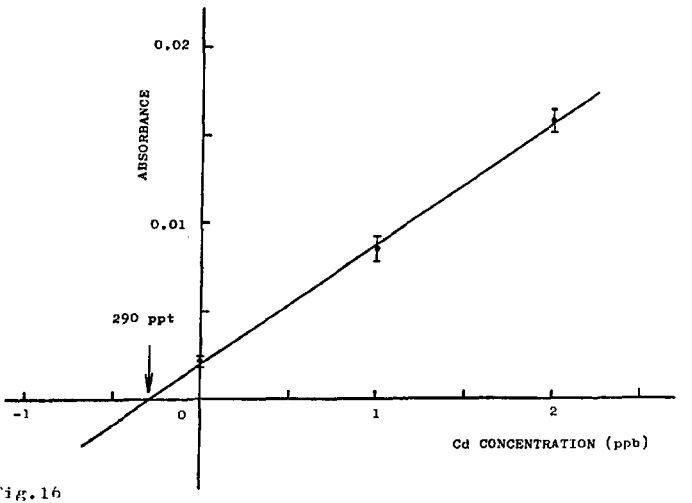
0.02
ABSORBANCE
0.01
290 ppt
-1
0
1
2
Cd CONCENTRATION (ppb)

Fig.16

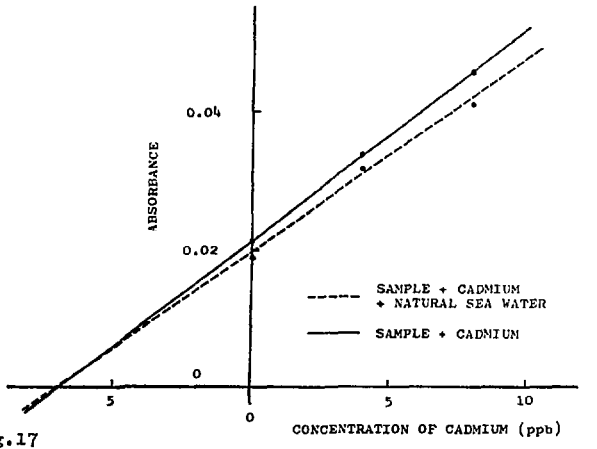
0.04
ABSORBANCE
0.02
SAMPLE + CADMIUM
+ NATURAL SEA WATER
SAMPLE + CADMIUM
0
5
0
5
10
CONCENTRATION OF CADMIUM (ppb)

Fig.17

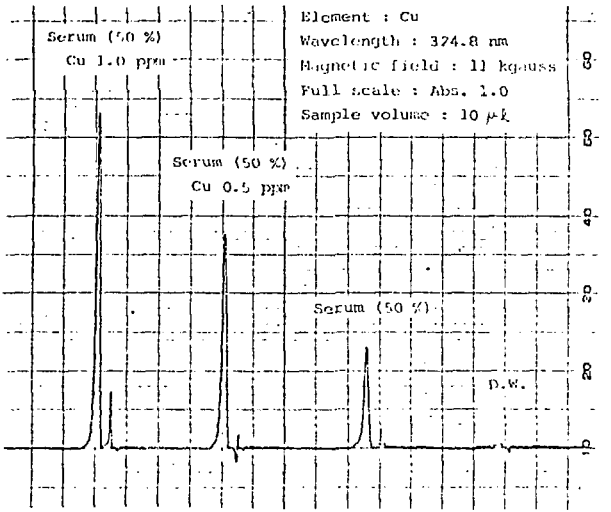
Element : Cu
Wavelength : 324.8 nm
Magnetic field : 11 kgauss
Full scale : Abs. 1.0
Sample volume : 10 μl
Serum (50 %)
Cu 1.0 ppm
Serum (50 %)
Cu 0.5 ppm
Serum (50 %)
D.W.

Fig.18

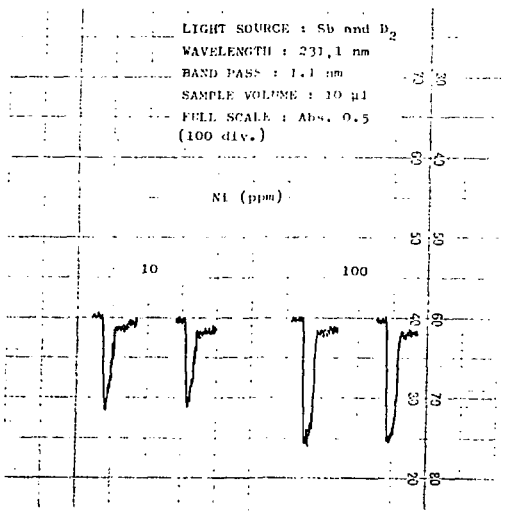
LIGHT SOURCE : Sb and D_2
WAVELENGTH : 231.1 nm
BAND PASS : 1.1 nm
SAMPLE VOLUME : 10 μl
FULL SCALE : Abs. 0.5
(100 div.)
Ni (ppm)
10
100

Fig.19

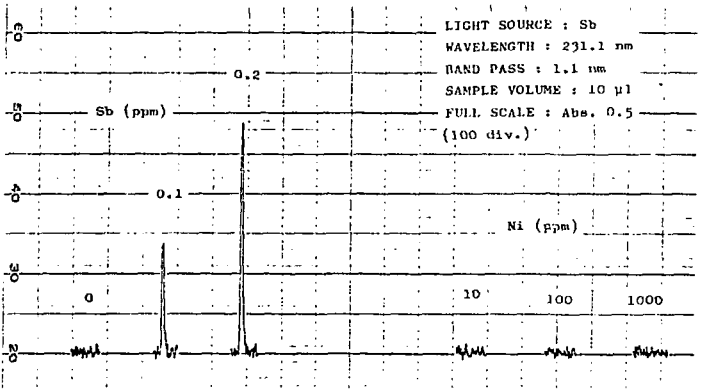
LIGHT SOURCE : Sb
WAVELENGTH : 231.1 nm
BAND PASS : 1.1 nm
SAMPLE VOLUME : 10 µl
FULL SCALE : Abs. 0.5
(100 div.)
0.2
Sb (ppm)
0.1
Ni (ppm)
0
10
100
1000

Fig.20

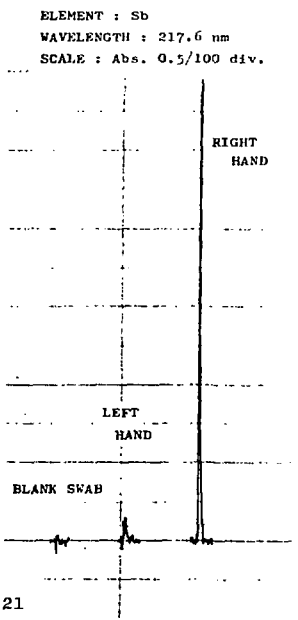
ELEMENT : Sb
WAVELENGTH : 217.6 nm
SCALE : Abs. 0.5/100 div.
RIGHT HAND
LEFT HAND
BLANK SWAB

Fig.21

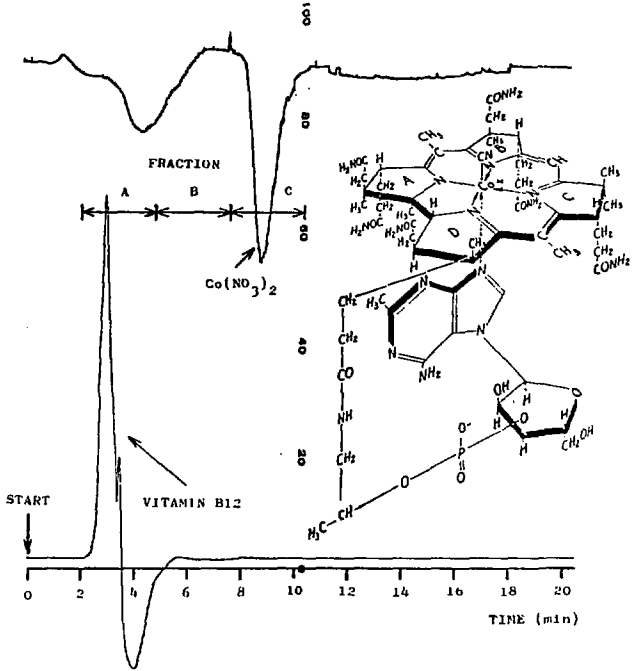
FRACTION
A
B
C
Co(NO3)2
START
VITAMIN B12
0
2
4
6
8
10
12
14
16
18
20
TIME (min)

Fig.22

a)

FRACTION A
(VITAMIN B12 PEAK)

ELEMENT : Co
WAVELENGTH : 240.7 nm
SAMPLE VOLUME : 10 µl
FULL SCALE : Abs. 0.25

VITAMIN B12

VITAMIN B12
+ $Co(NO_3)_2$

FRACTION (B)
(NO PEAK)

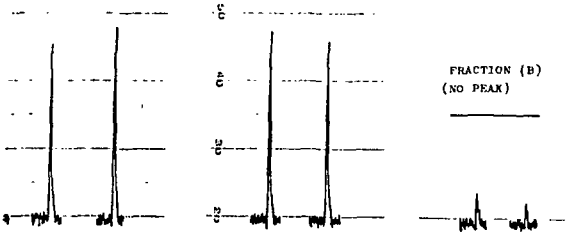

b)

FRACTION (C)
(INORGANIC Co PEAK)

VITAMIN B12
+ $Co(NO_3)_2$

ELEMENT : Co
WAVELENGTH : 240.7 nm
SAMPLE VOLUME : 5 µl
FULL SCALE : Abs. 0.5

VITAMIN B12

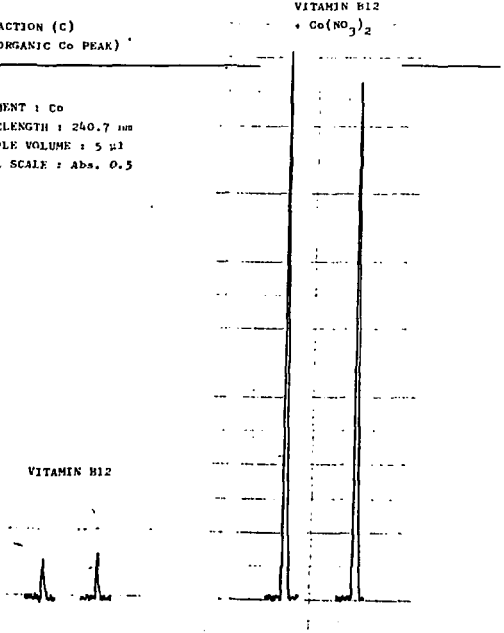

Fig.23